Thickness-driven polar spin reorientation transition in ultrathin Fe/Au(001) films

D. Wilgocka-Ślęzak,[1] K. Freindl,[1] A. Kozioł,[2] K. Matlak,[2] M. Rams,[3] N. Spiridis,[1] M. Ślęzak,[2] T. Ślęzak,[2] M. Zając,[2] and J. Korecki[1,2]

[1]*Institute of Catalysis and Surface Chemistry, Polish Academy of Sciences, Niezapominajek 8, 30-239 Cracow, Poland*

[2]*Department of Solid State Physics, AGH University of Science and Technology, Mickiewicza 30, 30-059 Cracow, Poland*

[3]*M. Smoluchowski Institute of Physics, Jagiellonian University, Reymonta 4, 30-059 Cracow, Poland*

(Received 9 June 2009; revised manuscript received 22 October 2009; published 22 February 2010)

The magnetic properties of ultrathin Fe films grown on Au(001) were studied at room temperature as a function of iron thickness in the range of two to three Fe monolayers (ML). The magneto-optic Kerr effect (MOKE) indicated that a spin reorientation from an in-plane direction to the film normal direction takes place when the iron thickness is reduced from 2.3 to 2.0 ML. Values of the effective magnetic anisotropy constants were determined from MOKE and superconducting quantum interference device measurements. The flow analysis of the effective anisotropy constants in anisotropy space revealed that the transition occurs via an intermediate state of canted magnetization.

DOI: 10.1103/PhysRevB.81.064421 PACS number(s): 75.70.−i, 75.30.Gw, 75.50.Bb

I. INTRODUCTION

Thickness-induced spin reorientation transitions (SRTs), which occur in many ultrathin ferromagnetic films, are of special interest not only for basic research but also for applications. The most common of these is the so-called "polar SRT," which is a spin reorientation from an in-plane direction to an out-of-plane direction that is observed when the film thickness is reduced below a critical value. Within a simplified picture, this spontaneous reorientation can be explained as the result of an outweighing of the thickness-dependent volume contribution to the effective anisotropy of the system by surface anisotropy, whose contribution increases with decreasing thickness. The volume part is dominated by a shape anisotropy that strongly supports magnetization parallel to the film plane, whereas the surface anisotropy (being a result of a broken local symmetry at the surface and/or at the interfaces) favors a perpendicular orientation, so that below a critical thickness, the effective anisotropy forces magnetization along the film normal direction. Such a situation is commonly referred in the literature as "perpendicular surface anisotropy." The effective anisotropy can be described by the well-known phenomenological expression proposed by Gradmann,[1]

$$K_1^{eff} = \tilde{K}_1^{V} + \frac{K_1^{S}}{t},$$

$$\tilde{K}_1^{V} = K_1^{V} - 2\pi M_s^2, \tag{1}$$

where K_1^S is the surface contribution (with dimensions of energy per unit surface), $\tilde{K}_1^V$ (energy per unit volume) is the volume contribution that includes the shape anisotropy term $(-2\pi M_s^2)$ and t is the film thickness. It has to be noted that, for a few monolayer thick films, a discrete approach to the shape anisotropy is necessary that results in additional contribution to the surface anisotropy K_1^S.[2] However, this is not essential for the present investigation, since in the paper we do not discuss separation of the magnetic anisotropy to the different contributions but we analyze the thickness dependence of the effective anisotropy constants. At the critical thickness, the volume and surface anisotropy contributions cancel each other, and the effective anisotropy is literally zero. According to the Mermin and Wagner theorem, in such a system at the critical point, long-range magnetic order should no longer be observed.[3] However, many experiments have shown (e.g., Refs. 4 and 5) that the SRT is influenced by higher-order anisotropy terms and that the behavior of the system in the vicinity of the critical thickness is controlled by the next nonvanishing contribution to the free-energy density.

Many experimental works have addressed the thickness-driven polar SRT phenomenon for various systems such as fcc Fe/Cu(001),[6–15] bcc Fe/Ag(001),[7,16–18] hcp Co/Au(111),[4,19–25] and many others (for a recent review, see Ref. 26). Although Fe/Au(001) and Fe/Ag(001) systems are similar in structure and although the SRT of silver-supported iron layers has been widely investigated, little attention has been given to the polar SRT within gold-supported iron films.[26,27] This situation most likely arises because for the Fe/Au(001) system, SRT is expected to occur at an extremely low thickness, which is difficult to experimentally investigate. Comparing the two systems, the room-temperature critical thickness for Fe/Ag(001) is around 7 monolayers (ML),[18] whereas for Fe/Au(001), it is below 3 ML.[27] This stems from the fact that the perpendicular interface anisotropy for iron on silver is nearly twice as large as that for iron on gold [0.81 and 0.47 ergs/cm^2, respectively, as compared to 0.96 ergs/cm^2 for Fe(001)/vacuum].[28] Although Brockmann *et al.* examined the Fe/Au(001) system as a function of the Fe thickness, that work concerned an in-plane SRT that is observed for thicker films, around 7 ML.[29] To the best of our knowledge, there has been only one previous work dedicated to the anisotropy study as a function of iron thickness for Fe/Au(001) in the polar-SRT thickness range.[27] Using the magneto-optic Kerr effect (MOKE), Liu *et al.* observed an in-plane easy axis even in the monolayer regime for Fe films grown at room temperature (earlier experiments showed the same—Refs. 30 and 31), whereas for the 100 K growth, the easy axis was along the film normal direction for films thinner than 2.8 ML. Since until now, no systematic

studies of the polar SRT for Fe/Au(001) have been undertaken, the present work was intended to complete this experimental gap.

Notwithstanding the lack of thorough studies of anisotropy, the Fe/Au(100) system has been a subject of numerous investigations concerning its structural, e.g., Refs. 32–43 and magnetic, e.g., Refs. 27, 29–31, 42, and 44–50 properties. It often plays a role as a model system for different theoretically predicted phenomena, such as the existence of ferromagnetism on an atomic level,[51] quantum wells,[52] or interlayer exchange coupling through a nonmagnetic spacer.[53–55] Fe monolayers grown on Au(001) have been cited as a model two-dimensional ferromagnet.[56] Fe films on Au(001) are only weakly strained due to the nearly perfect one to one lattice match of the bcc Fe(001) to fcc Au(001) lattice spacing (mismatch: 0.6%). The growth of Fe on Au(100) has been found to proceed via a layer-by-layer mode,[30] despite the unfavorable surface-energy relations between iron and gold. Due to the surface segregation of gold, the iron films are covered with a gold monolayer, which acts as a surfactant. It lowers the surface energy of the growing film and thereby prevents the formation of islands,[33,52,57] as has been confirmed by numerous experimental techniques over a wide thickness range.[33–41,52,57] On the other hand, the process of gold segregation is very sensitive to the preparation conditions (substrate temperature and deposition rate), which may lead to subtle differences in the morphology and composition of this apparently flat and perfect system.[42]

In the present paper, we report systematic investigations of the magnetic anisotropy of this system as a function of the Fe layer thickness around the polar SRT critical thickness, based mainly on MOKE measurements. This simple and well-established technique[58] has a surface sensitivity in the submonolayer range. The small area of the laser beam allows for studies of laterally inhomogeneous samples, which is extremely advantageous when experiments are carried out as a function of the film thickness. Instead of a series of samples, only one sample can be used in a MOKE experiment, with the thickness varying during a single preparation run in a continuous (a wedge form) or step fashion. In this way, the problem of irreproducibility of the deposition conditions is eliminated.

II. SAMPLE PREPARATION AND CHARACTERIZATION

Ultrathin Fe/Au(001) films were grown by molecular-beam epitaxy under ultrahigh-vacuum (UHV) conditions (base pressure below 1×10^{-10} mbar). Polished MgO(001) crystals, 1 mm thick, were used as substrates. A 200-Å-thick Au(001) buffer layer was deposited in a multistep process, as described in detail elsewhere.[39] The (001) orientation of gold was forced by a 40 Å Cr seed layer directly deposited at 100 °C on a thermally cleaned MgO substrate. On the Au(001) surface, iron was deposited at room temperature as a stepped film, with the Fe thickness changing from 2 to 3 ML (1 Fe ML is equivalent to 1.435 Å), e.g., in the thickness range of the expected spin reorientation transition. The thicknesses of the successive steps were 2.0, 2.3, 2.5, 2.7, and 3 ML, and their width was 2 mm. Additionally, a uniform reference sample with an Fe thickness of 3 ML was prepared. The uncertainty of the thickness as determined by quartz monitor indication was 0.1 ML. The as-deposited samples were covered with a gold protective layer (30 Å) to allow for *ex situ* measurements. The chemical purity of the sample surfaces and their structural order were controlled at each preparation step by Auger electron spectroscopy and by low-energy electron diffraction (LEED), respectively. The growth of iron could be characterized by scanning tunneling microscopy (STM) in a separate UHV system.[39]

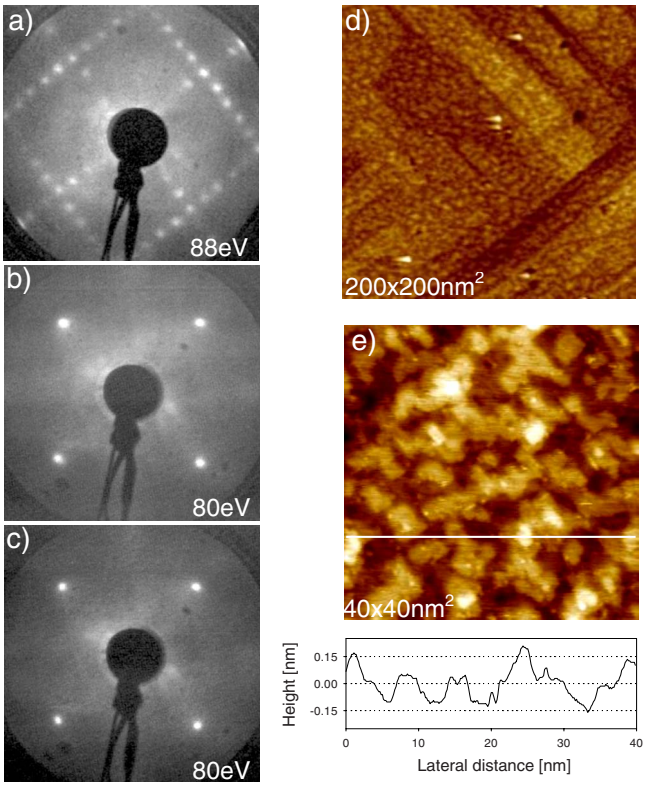

FIG. 1. (Color online) Right column: LEED patterns collected for: (a) Au(001) buffer layer, (b) 2.0 ML of Fe, and (c) 3.0 ML of Fe. The energy of the incident electron beam is given for each pattern. Left column: [(d) and (e)] topographic STM images for ~2.5 ML of Fe grown on Au(001) with cross section taken along white line.

The LEED pattern collected for the surface of the Au(001) buffer layer is shown in Fig. 1(a). The image indicates a high-quality, well-organized surface with typical (5 $\times$ 1) reconstruction. A detailed description of the so-called Au(001)-*hex* reconstructed surfaces, obtained via the same procedure, is presented elsewhere.[39] The Au reconstruction was lost during the subsequent deposition of iron at a coverage of about 0.6 Fe ML. Examples of diffraction patterns for 2.0 and 3.0 ML of Fe are shown in Figs. 1(b) and 1(c). LEED patterns collected from the stepped sample for the successive Fe thicknesses exhibited similar surface structures and good epitaxial quality for the in-plane Fe[100] direction parallel to Au[110]. However, increased diffusive background and distinct broadening of the diffraction spots at certain energies indicate an increased level of roughness, as compared to the Au substrate. Indeed, STM images for ~2.5 ML Fe, pre-

sented in Fig. 1, confirm this observation. The 200 $\times 200$ nm^2 topographic scan [Fig. 1(d)] shows that the surface of the iron film reflects topography of the gold substrate with characteristic monatomic step edges along ⟨110⟩ directions of Au. It is also seen that on the atomically flat Au terraces, tens-nanometer broad, Fe forms a much finer, nanometer-size inhomogeneities covering about 50% of the surface. At a higher magnification [Fig. 1(e), 40×40 nm^2] the inhomogeneities can be identified as roughness resulting from nucleation of small monatomic areas of the growing Fe film. A surface cross section marked by white line in Fig. 1(e) demonstrates vertical distances typical for monatomic Fe(001) steps (app. 0.15 nm) that corresponds to the height levels exposed during the growth of Fe. The growth is close to layer by layer. For the 2.5 ML film, the overwhelming surface contribution comes from two height levels, which means that the two-monolayer base of Fe is almost continuous. The average size of the lateral roughness resulting from noninteger number of layers and small deviation from the layer-by-layer growth is estimated as 5 nm. It should be noted that the presence of a gold monolayer on the imaged surface is plausible.[39]

The LEED images taken for the Au capping layer resembled the image of Fig. 1(a), indicating a structural coherence of the system. The *hex* reconstruction reappeared after the deposition of 2 Au ML.

III. MAGNETIC MEASUREMENTS AND DISCUSSION

The magnetic properties of the ultrathin Fe/Au(001) films were investigated as a function of thickness by observing the *ex situ* magneto-optical Kerr effect at room temperature with polar and longitudinal geometries. The light source was a He-Ne laser (632 nm) with a 0.1-mm-diameter light spot. To determine the saturation magnetization of the 3 ML Fe reference sample, superconducting quantum interference device (SQUID) measurements were carried out with an external magnetic field in the film plane and along the film normal direction.

Figure 2 presents the MOKE loops measured for the successive Fe thicknesses with the magnetic field applied in plane, along the Fe[100] direction (longitudinal geometry—right-hand side of Fig. 2), and out-of-plane (polar geometry—left-hand side of Fig. 2). The in-plane ⟨100⟩ directions of Fe was checked to be the iron easy magnetization directions for longitudinal geometry, in agreement with a Bader and Moog[30] work on Fe/Au(001) and bulk properties of iron as well. It is worth mentioning that in our investigations of the polar spin reorientation process the weak fourfold in-plane magnetic anisotropy could be neglected. As the Fe thickness decreases from 3.0 to 2.3 ML, the character of the loops does not change. Rectangular loops with full remanence magnetization in the longitudinal geometry, typical for an easy direction, and zero-remanence loops for the polar configuration indicate that the effective anisotropy is dominated by the in-plane anisotropy for this thickness range. According to the commonly used sign convention for the free-energy density, $E_a = -K_1^{eff} \cos^2 \theta$ (θ is the magnetization polar angle), the effective anisotropy constant K_1^{eff}, in

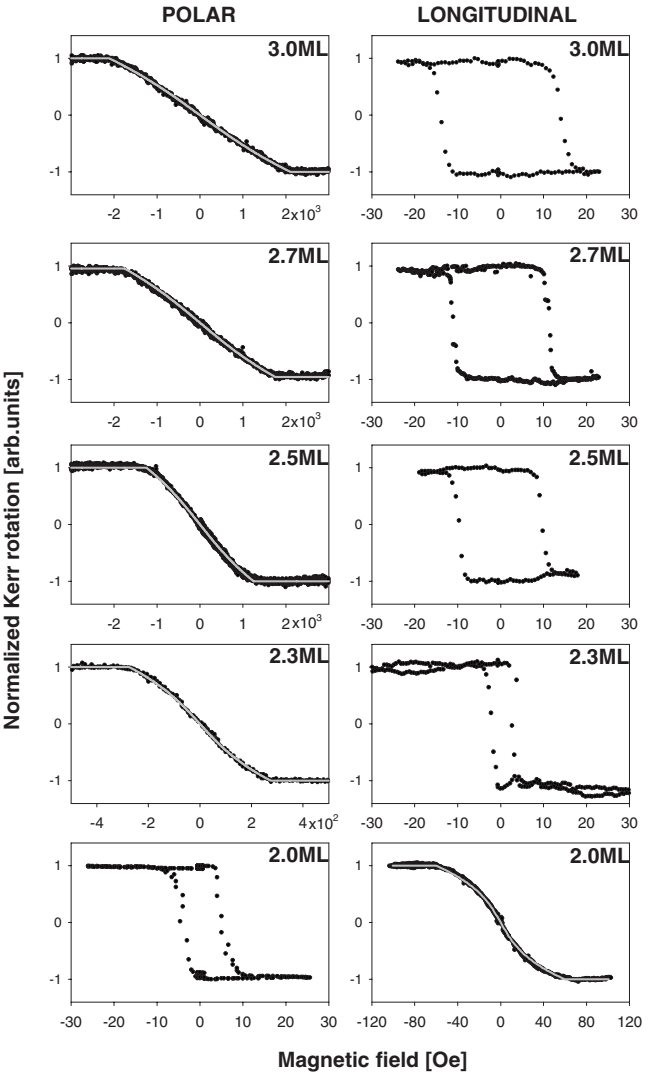

FIG. 2. Polar and longitudinal MOKE loops measured in the range of the spin reorientation transition for successive iron thicknesses between 3.0 and 2.0 ML. The hard loops are presented with corresponding simulated curves.

the case of in-plane easy axis, is negative. For this thickness range, the negative shape anisotropy dominates. The absolute value of K_1^{eff} gradually diminishes as the Fe layer thickness decreases, as a result of an increasing positive surface contribution that favors out-of-plane magnetization. This effect is manifested by a decrease in the anisotropy field H_a (the magnetic field that saturates sample along a hard direction) with decreasing film thickness, which is shown in Fig. 3. A reduction in the film thickness by less than 1 ML reduces the in-plane saturation field by nearly 1 order of magnitude, as seen in Table I.

For 2.0 ML of Fe, the MOKE measurements show a qualitative change with respect to the data taken for thicker films. An easy loop for out-of-plane and a hard loop for in-plane field configurations indicate that the easy axis in this case points along the film normal and that the effective anisotropy constant is now positive. This means that the spin reorientation transition from in plane to out of plane for Fe/

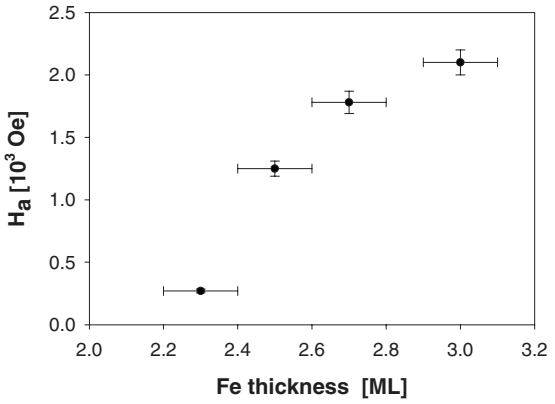

FIG. 3. Anisotropy field H_a derived from the hard-axis MOKE loops as a function of the nominal Fe layer thickness.

Au(001) takes place in the thickness range between 2.0 and 2.3 ML.

Simulations of the magnetization loops that best reproduce the measured hard loops enabled a quantitative determination of the anisotropy constants of the investigated system. In order to reproduce the shape of the experimental curves, a higher order of the effective anisotropy constant K_2^{eff}, defined analogously to K_1^{eff}, compare Eq. (1) had to be taken into account. The simulations were based on a simple one-domain model, in which a magnetic layer is described by saturation magnetization M_s and effective anisotropy constants K_1^{eff} and K_2^{eff}. By minimizing the density of the free energy,

$$E(\theta) = -M_s H \cos(\theta - \theta_H) - K_1^{eff} \cos^2 \theta - K_2^{eff} \cos^4 \theta \tag{2}$$

the equilibrium configuration θ of the layer magnetization was determined as a function of the magnetic field H. The angles in Eq. (2) are polar angles and θ_H indicates the direction of the applied magnetic field. In the simulations, M_s was treated as fixed parameter. It should be noted that this procedure can find local energy minima, which allowed hysteretic loops to be obtained.

The value of the saturation magnetization M_s for the 3 ML Fe film was determined experimentally from the reference sample via SQUID measurements for both field configurations. The results of the SQUID magnetometry are shown in Fig. 4, yielding the value of $M_s = 1000 \pm 80$ emu/cm^3. To estimate the M_s values for thinner Fe films, we used a linear $M_s(t)$ dependence, assuming, for films between 3.0 and 2.0 ML, a slope of -250 ± 20 emu cm^{-3} Å^{-1}, in agreement with our Mössbauer data[42,59] and with magnetization measurements for the [Fe(t Å)/Au(12 Å)]$_{40}$ system by Honda *et al.*[47] Estimates of the M_s values for the iron thicknesses under discussion are listed in Table I.

TABLE I. Saturation magnetization M_s, anisotropy constants K_1^{eff} and K_2^{eff}, and anisotropy field H_a for decreasing thickness of iron films on Au(001)-*hex*. $H_a^{\perp} = \left|\frac{2K_1+4K_2}{M_s}\right|$ $H_a^{\parallel} = \frac{2K_1}{M_s}$. The symbols $\perp$ and $\parallel$ represent the magnetic field orientation perpendicular and parallel to the film surface, respectively.

t_{Fe} (ML)	M_s (emu/cm^3)	K_1^{eff} (erg/cm^3)	K_2^{eff} (erg/cm^3)	H_a (Oe)
3.0	1000 ± 80	$-91 \pm 10 \times 10^4$	$-7.0 \pm 0.8 \times 10^4$	$2100 \pm 100 \perp$
2.7	884 ± 166	$-67 \pm 15 \times 10^4$	$-6.0 \pm 1.3 \times 10^4$	$1780 \pm 90 \perp$
2.5	806 ± 171	$-42 \pm 11 \times 10^4$	$-4.0 \pm 1.0 \times 10^4$	$1250 \pm 60 \perp$
2.3	729 ± 177	$-7.1 \pm 2.0 \times 10^4$	$-1.30 \pm 0.37 \times 10^4$	$270 \pm 15 \perp$
2.0	613 ± 186	$+1.7 \pm 0.5 \times 10^4$	$-0.40 \pm 0.12 \times 10^4$	$55 \pm 3 \parallel$

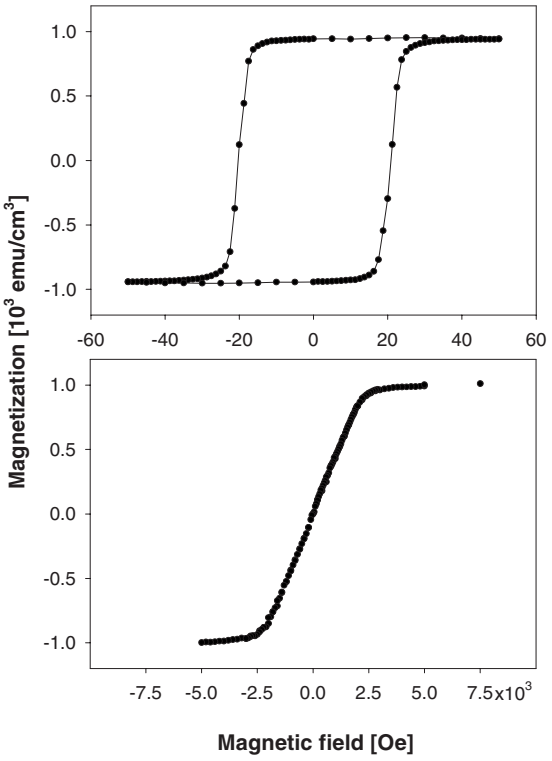

FIG. 4. SQUID magnetization loops for 3 ML of Fe measured at room temperature for in-plane (upper panel) and out-of-plane (lower panel) magnetic field configurations.

Values of the anisotropy constants K_1^{eff} and K_2^{eff} obtained from the aforementioned simulations of the hard direction MOKE curves are also shown in Table I. The experimental and simulated curves are compared in Fig. 2. The necessity of taking into account a higher-order contribution to the anisotropy energy indicates that the SRT in the Fe/Au(001) system is not a simple magnetization switching between the in- and out-of-plane configurations but must be much a more complex process.

In this case, following Millev and Kirschner[60] and Oepen *et al.*,[4] the SRT problem can be elegantly analyzed in the anisotropy space that is spanned by the anisotropy constants K_1^{eff} and K_2^{eff}. Minimization of the anisotropy free energy,

$$E_a = -K_1^{eff} \cos^2 \theta - K_2^{eff} \cos^4 \theta + \cdots \tag{3}$$

with respect to θ distinguishes three magnetization states: (i) with perpendicular ($\theta = 0$), (ii) in plane ($\theta = \pi/2$), and (iii) canted easy axes ($\theta \neq 0, \pi/2$). An analysis of the SRT in

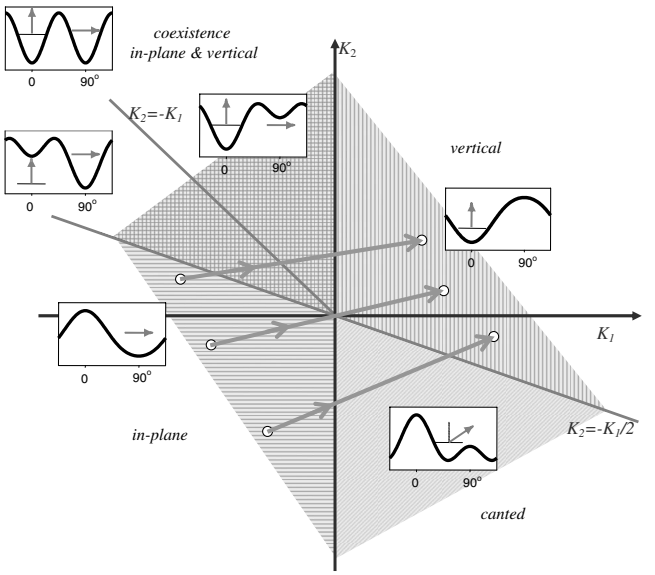

FIG. 5. Anisotropy space spanned by the anisotropy constants K_1^{eff} and K_2^{eff} (after Refs. 3 and 59). Areas marked by horizontal, vertical, canted, and criss-crossed lines correspond to phases with spontaneous in-plane, perpendicular, and canted magnetizations and to phases of coexistence, respectively. The insets show energy dependencies on the angle θ characteristic for the distinguished regions. The straight lines (with arrows) across the anisotropy space represent three possible scenarios of the spin reorientation transition for a linear thickness-driven evolution of anisotropy constants: (1) through the point with zero anisotropy, (2) through a canted phase, and (3) through the area of phase coexistence.

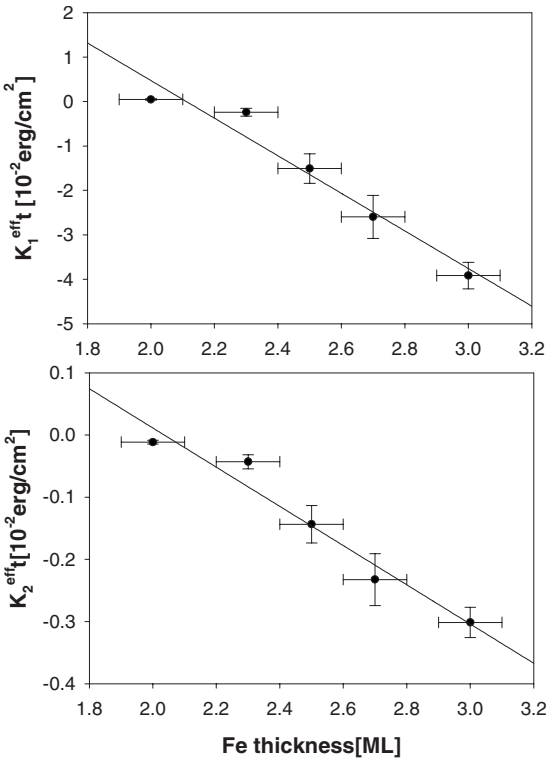

FIG. 6. The values of $K_1^{eff}t$ and $K_2^{eff}t$ obtained from the fitted hard-axis MOKE loops and corresponding linear regressions (straight lines) as a function of the Fe layer thickness t.

anisotropy space is shown in Fig. 5. For positive K_1^{eff}, the magnetization is perpendicular when $K_2^{eff} > -\frac{1}{2}K_1^{eff}$ or canted when $K_2^{eff} < -\frac{1}{2}K_1^{eff}$. For negative K_1^{eff} values there is an in-plane magnetization phase for $K_2^{eff} < -\frac{1}{2}K_1^{eff}$, while for $K_2^{eff} > -\frac{1}{2}K_1^{eff}$, the perpendicular and in-plane magnetization phases coexist as a consequence of two local minima for the anisotropy energy given by Eq. (3).

K_1^{eff} and K_2^{eff} depend on the layer thickness t, and changes in this driving parameter between the initial and final state force the system to evolve along a specific trajectory in anisotropy space (so-called thickness-driven anisotropy flow[4,60]). When Gradmann's relation [Eq. (1)] for K_1^{eff} and K_2^{eff} holds, the trajectory is linear and there are three possible scenarios for the SRT, as shown in Fig. 5: (1) trivial (but rare), through the origin of anisotropy space, (2) through a canted phase with an easy magnetization cone, and (3) through the coexistence of perpendicular and in-plane phases. Provided that the effective anisotropy constants have been experimentally determined, the SRT type can be derived by means of anisotropy space analysis.

It must be noted that the phenomenological Gradmann's relations [Eq. (1)] for K_1^{eff} and K_2^{eff} are not directly applicable to films in the range of a few monolayers, and in our case, the determination of the surface and volume anisotropy constants K_S and K_V has no physical meaning. However, a linear dependence of $K_1^{eff}t$ and $K_2^{eff}t$ on t should be expected when taking into account the following arguments: (i) the considered Fe thickness range is only 1 monolayer (2.0–3.0 ML), (ii) a film with a fractional number of monolayers is actually realized (for ideal layer-by-layer growth) as a combination of layers with two consecutive integer numbers of monolayers, and hence, (iii) the anisotropy energy per unit surface for a film with a fractional number of monolayers is a weighted average of the values for the two layers consisting of the integer numbers of monolayers, and by simple arguments (within a single-monolayer thickness range), it scales with the actual film thickness. The experimental dependencies of $K_1^{eff}t$ and $K_2^{eff}t$ on t are shown in Fig. 6. Indeed, they can be best fitted by straight lines, evidencing the layer-by-layer Fe growth promoted by the surfactant role of gold.

Finally, Fig. 7 shows the anisotropy constants for successive iron thicknesses plotted in anisotropy space (K_1^{eff}, K_2^{eff}). Such a representation is free from errors of thickness determination. Obviously, the points lie on a straight line as a consequence of the linear dependence of $K_1^{eff}t$ and $K_2^{eff}t$ on t. The trajectory displays the mechanism of the thickness-driven SRT, showing that it occurs via a very narrow area of the easy cone state.

Explanation of the microscopic origin of higher-order anisotropy term is beyond our phenomenological treatment of the problem. We can only speculate that K_2^{eff} (regardless of its volume or surface nature) originates mainly from lateral inhomogeneities connected with the effect of noninteger thickness superimposed on the atomic-scale roughness arising from the deviations from the layer-by-layer growth.

Such lateral inhomogeneities can lead to coexistence of areas with opposing magnetic tendencies due to different

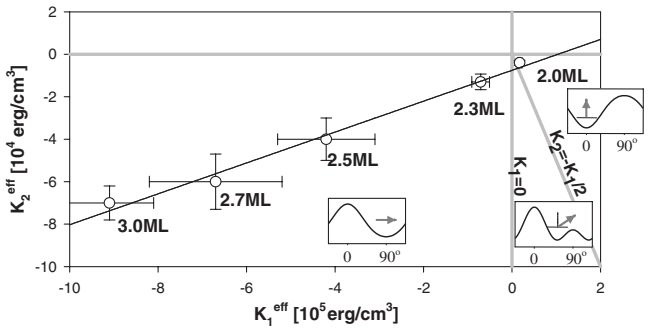

FIG. 7. Experimental values of K_1^{eff} and K_2^{eff} plotted in anisotropy space for Fe layers in the thickness range of 2.0–3.0 ML. The straight line through the experimental points corresponds to the thickness-driven evolution of the anisotropy constants and indicates that the SRT from the in-plane to out-of-plane easy direction occurs via the area of a canted phase. The insets show the character of the anisotropy energy for the respective areas of the anisotropy space.

thicknesses of these regions. As in our case, for 2 ML areas, local anisotropy favors out-of-plane magnetic order whereas for 3-ML-thick Fe patches, an in-plane easy axis is expected. In such a system, if the lateral scale of the local film thickness inhomogeneities is smaller than the exchange length [~20 nm for Fe (Ref. 26)], the canting of the magnetic moments, and not the phase coexistence, is the way to lower the total magnetic energy. The canting can be accompanied by deviations from collinear order, understood as certain angular distribution of the magnetization direction around an average canting angle.[26] As it was calculated by Jensen *et al.*, such noncollinearities contribute to K_2^{eff} with always negative sign favoring continuous polar SRT.[26] It should be noted that noncollinear order has collective character and a phase with a strictly perpendicular magnetization in some parts of the system, and a canted or an in-plane one in other parts, does not exist. In case of the investigated films the average scale of lateral roughness derived from the STM studies is of nanometer size while the vertical one compares to the interatomic distances in Fe(001). According to Jensen's calculation for such roughness parameters the angle difference between magnetic moments of neighboring Fe areas is small (smaller than a few degrees) (Ref. 26) and thus, the system can be treated as a collinear one, described by an angle which is the average throughout all the spins.

IV. CONCLUSIONS

A perpendicular anisotropy was detected for the room-temperature grown ultrathin Fe films on Au(001) *hex*. MOKE measurements showed that the thickness-induced SRT in this system is not a simple process, which takes place for a discrete Fe thickness when the first-order effective anisotropy constant zeros ($K_1^{eff}=0$) but it is driven by higher terms of anisotropy and undergoes gradually, nonetheless in a narrow thickness range between 2.3 and 2.0 ML in the presence of an intermediate state. The numerical analysis of the experimental MOKE and SQUID magnetization curves gave a precise determination of the thickness dependence of the anisotropy constants K_1^{eff} and K_2^{eff}. The interpretation of the SRT in the anisotropy space enabled unambiguous selection between various SRT scenarios and revealed that the transition undergoes through an easy cone magnetization state. The origin of the intermediate canted magnetization state that is concluded from the experiment can be attributed to lateral structural inhomogeneities that arises from noninteger number of the investigated layers and small deviations from the layer-by-layer growth. Due to existence of areas with specific thicknesses that trigger contrary magnetic local anisotropies a canted order emerges.

ACKNOWLEDGMENTS

This work was supported in part by the Polish Ministry of Science and Higher Education and by the Team Program of the Foundation for Polish Science co-financed by the EU European Regional Development Fund.

[1] U. Gradmann and J. Mueller, Phys. Status Solidi **27**, 313 (1968).
[2] H. J. G. Draaisma and W. J. M. de Jonge, J. Appl. Phys. **64**, 3610 (1988).
[3] N. D. Mermin and H. Wagner, Phys. Rev. Lett. **17**, 1133 (1966).
[4] H. P. Oepen, M. Speckmann, Y. Millev, and J. Kirchner, Phys. Rev. B **55**, 2752 (1997).
[5] J.-W. Lee, J.-R. Jeong, S.-Ch. Shin, J. Kim, and S.-K. Kim, Phys. Rev. B **66**, 172409 (2002).
[6] C. Liu, E. R. Moog, and S. D. Bader, Phys. Rev. Lett. **60**, 2422 (1988).
[7] D. P. Pappas, C. R. Brundle, and H. Hopster, Phys. Rev. B **45**, 8169 (1992).
[8] J. Thomassen, F. May, B. Feldmann, M. Wuttig, and H. Ibach, Phys. Rev. Lett. **69**, 3831 (1992).
[9] R. Allenspach and A. Bischof, Phys. Rev. Lett. **69**, 3385 (1992).
[10] D. Li, M. Freitag, J. Pearson, Z. Qiu, and S. Bader, Phys. Rev. Lett. **72**, 3112 (1994).
[11] M. T. Lin, J. Shen, W. Kuch, H. Jenniches, M. Klaua, C. M. Schneider, and J. Kirschner, Phys. Rev. B **55**, 5886 (1997).
[12] S. S. Kang, W. Kuch, and J. Kirschner, Phys. Rev. B **63**, 024401 (2000).
[13] M. A. Torija, J. P. Pierce, and J. Shen, Phys. Rev. B **63**, 092404 (2001).
[14] P. Castrucci, R. Gunnella, R. Bernardini, P. Falconi, and M. De Crescenzi, Phys. Rev. B **65**, 235435 (2002).
[15] D. Peterka, A. Enders, G. Haas, and K. Kern, Phys. Rev. B **66**, 104411 (2002).
[16] N. C. Koon, B. T. Jonker, F. A. Volkening, J. J. Krebs, and G. A. Prinz, Phys. Rev. Lett. **59**, 2463 (1987).
[17] J. Araya-Pochet, C. A. Ballentine, and J. L. Erskine, Phys. Rev. B **38**, 7846 (1988).
[18] Z. Qiu, J. Pearson, and S. Bader, Phys. Rev. Lett. **70**, 1006 (1993).
[19] R. Allenspach, M. Stampanoni, and A. Bischof, Phys. Rev. Lett.

65, 3344 (1990).
[20] S. Pütter, H. F. Ding, Y. T. Millev, H. P. Oepen, and J. Kirschner, Phys. Rev. B **64**, 092409 (2001).
[21] H. F. Ding, S. Pütter, H. P. Oepen, and J. Kirschner, Phys. Rev. B **63**, 134425 (2001).
[22] L. Cagnon, T. Devolder, R. Cortes, A. Morrone, J. E. Schmidt, and C. Chappert, Phys. Rev. B **63**, 104419 (2001).
[23] R. Sellmann, H. Fritzsche, H. Maletta, V. Leiner, and R. Siebrecht, Phys. Rev. B **64**, 054418 (2001).
[24] J. Langer, J. Hunter Dunn, A. Hahlin, O. Karis, R. Sellmann, D. Arvanitis, and H. Maletta, Phys. Rev. B **66**, 172401 (2002).
[25] M. Kisielewski, A. Maziewski, M. Tekielak, A. Wawro, and L. T. Baczewski, Phys. Rev. Lett. **89**, 087203 (2002).
[26] P. J. Jensen and K. H. Bennemann, Surf. Sci. Rep. **61**, 129 (2006).
[27] C. Liu and S. D. Bader, J. Vac. Sci. Technol. A **8**, 2727 (1990).
[28] B. Heinrich, Z. Celiński, J. F. Cochran, A. S. Arrott, and K. Myrtle, J. Appl. Phys. **70**, 5769 (1991).
[29] M. Brockmann, S. Miethaner, R. Onderka, M. Köohler, F. Himmelhuber, H. Regensburger, M. Bensch, T. Schweinböck, and G. Bayreuther, J. Appl. Phys. **81**, 5047 (1997).
[30] S. Bader and E. R. Moog, J. Appl. Phys. **61**, 3729 (1987).
[31] W. Dürr, M. Taborelli, O. Paul, R. Germar, W. Gudat, D. Pescia, and M. Landolt, Phys. Rev. Lett. **62**, 206 (1989).
[32] Q. Jiang, Y. L. He, and G. C. Wang, Surf. Sci. **295**, 197 (1993).
[33] Y. L. He and G. C. Wang, Phys. Rev. Lett. **71**, 3834 (1993).
[34] C. J. Pastor, C. Limones, J. J. Hinarejos, J. M. Garcia, R. Miranda, J. Gomez-Goni, J. Ortega, and H. D. Abruna, Surf. Sci. **364**, L505 (1996).
[35] R. Opitz, S. Lobos, A. Thissen, and R. Courths, Surf. Sci. **370**, 293 (1997).
[36] O. S. Hernán, A. L. Vázquez de Parga, J. M. Gallego, and R. Miranda, Surf. Sci. **415**, 106 (1998).
[37] O. S. Hernán, J. M. Gallego, A. L. Vázquez de Parga, and R. Miranda, Appl. Phys. A: Mater. Sci. Process. **66**, S1117 (1998).
[38] S. A. Kellar, Y. Chen, W. R. A. Huff, E. J. Moler, Z. Hussain, and D. A. Shirley, Phys. Rev. B **57**, 1890 (1998).
[39] N. Spiridis and J. Korecki, Appl. Surf. Sci. **141**, 313 (1999).
[40] V. Blum, Ch. Rath, S. Müller, L. Hammer, K. Heinz, J. M. García, J. E. Ortega, J. E. Prieto, O. S. Hernán, J. M. Gallego, A. L. Vázquez de Parga, and R. Miranda, Phys. Rev. B **59**, 15966 (1999).
[41] R. Belkhou, R. Flammini, M. Marsi, A. Taleb-Ibrahimi, L. Gregoratti, A. Barinov, and M. Kiskinova, Surf. Sci. **532-535**, 63 (2003).
[42] W. Karaś, B. Handke, K. Krop, M. Kubik, T. Ślęzak, N. Spiridis, D. Wilgocka-Ślęzak, and J. Korecki, Phys. Status Solidi A **189**, 287 (2002).
[43] N. Spiridis and J. Korecki, Surf. Sci. **507-510**, 135 (2002).
[44] H. Yamazaki, Phys. Status Solidi B **197**, 195 (1996).
[45] K. Takanashi, S. Mitani, M. Sano, and H. Fujimori, Appl. Phys. Lett. **67**, 1016 (1995).
[46] K. Takanashi, S. Mitani, H. Fujimori, K. Sato, and Y. Suzuki, J. Magn. Magn. Mater. **177-181**, 1199 (1998).
[47] S. Honda, K. Koguma, M. Nawate, and I. Sakamoto, J. Appl. Phys. **82**, 4428 (1997).
[48] K. Sato, T. Kondo, J. Abe, H. Ikekame, M. Sano, S. Mitani, K. Takanashi, and H. Fujimori, J. Magn. Soc. Jpn. **20**, 197 (1996).
[49] S. Riedling, N. Knorr, C. Mathieu, J. Jorzick, S. O. Demokritov, B. Hillebrands, R. Schreiber, and P. Grünberg, J. Magn. Magn. Mater. **198-199**, 348 (1999).
[50] L. Uba, S. Uba, V. N. Antonov, A. N. Yaresko, T. Slezak, and J. Korecki, Phys. Rev. B **62**, 13731 (2000).
[51] S. De Rossi, F. Ciccacci, and S. Crampin, Phys. Rev. B **52**, 3063 (1995).
[52] F. J. Himpsel, Phys. Rev. B **44**, 5966 (1991).
[53] A. Fuß, S. O. Demokritov, P. Grünberg, and W. Zinn, J. Magn. Magn. Mater. **103**, L221 (1992).
[54] J. Unguris, R. J. Celotta, and D. T. Pierce, J. Appl. Phys. **75**, 6437 (1994).
[55] J. Unguris, R. J. Celotta, and D. T. Pierce, Phys. Rev. Lett. **79**, 2734 (1997).
[56] F. J. Himpsel, J. E. Ortega, G. J. Mankey, and R. F. Willis, Adv. Phys. **47**, 511 (1998).
[57] A. M. Begley, S. K. Kim, J. Quinn, F. Jona, H. Over, and P. M. Marcus, Phys. Rev. B **48**, 1779 (1993).
[58] Z. Q. Qiu and S. D. Bader, Rev. Sci. Instrum. **71**, 1243 (2000).
[59] T. Ślęzak and J. Korecki (unpublished).
[60] Y. Millev and J. Kirschner, Phys. Rev. B **54**, 4137 (1996).